

Anyonic Haldane insulator in one dimension

Florian Lange,^{1,2} Satoshi Ejima,² and Holger Fehske²

¹*Computational Condensed Matter Physics Laboratory, RIKEN, Wako, Saitama 351-0198, Japan*

²*Institut für Physik, Ernst-Moritz-Arndt-Universität Greifswald, 17489 Greifswald, Germany*

(Dated: December 5, 2016)

We demonstrate numerically the existence of a nontrivial topological Haldane phase for the one-dimensional extended (U - V) Hubbard model with a mean density of one particle per site, not only for bosons but also for anyons, despite a broken reflection parity symmetry. The Haldane insulator, surrounded by superfluid, Mott insulator and density-wave phases in the V - U parameter plane, is protected by combined (modified) spatial-inversion and time-reversal symmetries, which is verified within our matrix-product-state based infinite density-matrix renormalization group scheme by analyzing generalized transfer matrices. With regard to an experimental verification of the anyonic Haldane insulator state the calculated asymmetry of the dynamical density structure factor should be of particular importance.

Anyons represent a third fundamental class of particles with fractional exchange statistics that interpolates, to some degree, between those of bosons and fermions having symmetric or antisymmetric wave functions under exchange [1, 2]. By contrast, the exchange of two anyons creates a phase factor $e^{i\theta}$ in the many-body wave function, where the statistical parameter θ can be of any value in the interval $(0, \pi)$. In the beginning anyons were thought to be relevant solely for two-dimensional systems. Describing the fractional quantum Hall effect experiments in particular, the quasiparticles could be viewed as anyons with θ fixed by the filling factor [3, 4]. With Haldane's generalized Pauli principle and definition of fractional statistics, however, the concept of anyons becomes important in arbitrary dimensions [5].

In one dimension, the physics of anyons might be studied successfully with ultra-cold atoms in optical lattices [6]. For example, Keilmann *et al.* proposed that anyon statistics in one-dimensional (1D) lattices can be implemented by bosons with occupation-dependent hopping amplitudes generated by assisted Raman tunneling [7], an approach that subsequently was refined by Greschner and Santos [8]. An alternative route to create 1D anyons in an optical lattice has been put forward by Sträter *et al.* [9] quite recently. Their scheme exploits lattice-shaking-assisted tunneling against potential offsets generated by a combination of a static potential tilt and strong on-site interactions. Thereby, advantageously, no additional lasers are required, except for those employed on creating optical lattices. However, in spite of the huge experimental efforts, a conclusive detection of 1D anyons in optical lattices has not yet been achieved.

Notwithstanding, from a theoretical point of view, anyons in one dimension received a continuous and legitimate interest on account of their intriguing physical properties. Using the Bethe ansatz technique Kundu obtained the exact solution of an 1D anyon gas with delta-function potential [10]. In the framework of the anyon-Hubbard model (AHM) on a 1D lattice, the possibility of a statistically induced quantum phase transition between

Mott-insulator (MI) and superfluid (SF) phases [7, 11] and the asymmetry of the momentum distribution for hard-core [12] and soft-core anyons [13] have been addressed so far. Since the AHM is equivalent to a variant of the Bose-Hubbard model (BHM) with state-dependent bosonic hopping amplitudes [7], the next very interesting question might be whether the symmetry-protected topological Haldane state [14, 15], observed in the extended BHM (EBHM) with an additional nearest-neighbor particle repulsion [16, 17], also shows up in the extended AHM (EAHM). As the hopping phase factor breaks reflection parity in the system [18], at first glance one would expect the Haldane state to disappear in the EAHM for any finite fractional phase θ . Perhaps surprisingly, this does not necessarily need to happen.

To examine the possibility of a topological Haldane state in one dimension, in this Letter, we study the EAHM using the matrix-product-state (MPS) based density-matrix renormalization-group (DMRG) technique [19, 20]. Considering the invariance of the density-dependent hopping amplitudes and calculating generalized transfer matrices [21] from the infinite MPS (iMPS) of the infinite DMRG (iDMRG) simulations [22], we can determine the protecting symmetry of the Haldane state and derive the complete ground-state phase diagram of this paradigmatic anyonic model Hamiltonian. In order to discriminate the topological Haldane insulator (HI) from the other, more conventional Mott (MI) and density-wave (DW) phases in possible future experiments, we will also analyze the dynamical density response of the system, showing a characteristic asymmetry in the Brillouin zone, which can be attributed to the fractional phase factor of the anyons.

The Hamiltonian of the 1D EAHM consists of three terms, $\hat{H}_{\text{EAHM}}^{(a)} \equiv \hat{H}_t + \hat{H}_U + \hat{H}_V$, with

$$\hat{H}_t = -t \sum_j \left(\hat{a}_j^\dagger \hat{a}_{j+1} + \text{h.c.} \right), \quad (1)$$

$\hat{H}_U = U \sum_j \hat{n}_j (\hat{n}_j - 1)/2$ and $\hat{H}_V = V \sum_j \hat{n}_j \hat{n}_{j+1}$, describing the nearest-neighbor anyon transfer ($\propto t$), as

well as the repulsive on-site ($\propto U$) and nearest-neighbor ($\propto V$) particle interaction, respectively. The anyon creation (\hat{a}_j^\dagger), annihilation (\hat{a}_j) and particle number ($\hat{n}_j = \hat{a}_j^\dagger \hat{a}_j$) operators at lattice site j are defined by the generalized commutation relations [7, 10]:

$$\hat{a}_j \hat{a}_\ell^\dagger - e^{-i\theta \text{sgn}(j-\ell)} \hat{a}_\ell^\dagger \hat{a}_j = \delta_{j\ell}, \quad (2)$$

$$\hat{a}_j \hat{a}_\ell - e^{i\theta \text{sgn}(j-\ell)} \hat{a}_\ell \hat{a}_j = 0, \quad (3)$$

where the sign function $\text{sgn}(j-k) = 0$ for $j=k$ is mandatory, since two anyons on the same site behave as ordinary bosons. Anyons with $\theta = \pi$ represent so-called “pseudofermions”, namely, they are fermions off-site, while being bosons on-site.

Implementing a fractional Jordan–Wigner transformation [7],

$$\hat{a}_j = \hat{b}_j e^{i\theta \sum_{\ell=1}^{j-1} \hat{n}_\ell}, \quad (4)$$

where \hat{b}_j^\dagger (\hat{b}_j) is a boson creation (annihilation) operator, $\hat{H}_{\text{EAHM}}^{(a)} \rightarrow \hat{H}_{\text{EAHM}}^{(b)}$ with density-dependent hopping amplitudes,

$$\hat{H}_t = -t \sum_j \left(\hat{b}_j^\dagger \hat{b}_{j+1} e^{i\theta \hat{n}_j} + e^{-i\theta \hat{n}_j} \hat{b}_{j+1}^\dagger \hat{b}_j \right). \quad (5)$$

That is when a boson hops to the left from site $j+1$ to site j it acquires a occupation dependent phase $e^{i\theta \hat{n}_j}$. Of course, $\hat{n}_j = \hat{a}_j^\dagger \hat{a}_j = \hat{b}_j^\dagger \hat{b}_j$, which means that \hat{H}_U and \hat{H}_V are form-invariant under the anyon-boson mapping (4).

If we limit the maximum number of particles per site as $n_p = 2$, the EBHM, resulting in the limit $\theta \rightarrow 0$ from $\hat{H}_{\text{EAHM}}^{(b)}$, maps to an effective XXZ spin-1 chain model [17]:

$$\begin{aligned} \hat{H}_{\text{eff}} = & -t \sum_j \left(\hat{S}_j^+ \hat{S}_{j+1}^- + \text{h.c.} \right) + \frac{U}{2} \sum_j \left(\hat{S}_j^z \right)^2 \\ & + V \sum_j \hat{S}_j^z \hat{S}_{j+1}^z \end{aligned} \quad (6)$$

with the pseudospin operator $\hat{S}_j^z = \hat{n}_j - 1$. Here, we have neglected terms which break the particle-hole symmetry. Note the negative sign of the first term compared to the usual XXZ spin-chain Hamiltonian. This leads to a protecting modified inversion symmetry (\mathcal{I}') for the Haldane state of the EBHM [15]:

$$\mathcal{I}' = e^{i\pi \sum_j \hat{S}_j^z} \mathcal{I} = e^{i\pi \sum_j (\hat{n}_j - 1)} \mathcal{I}. \quad (7)$$

Owing to the occupation-dependent hopping in (5) the HI phase in the EAHM seems not be protected by the modified inversion symmetry \mathcal{I}' .

To clarify whether \hat{H}_t is invariant under certain symmetry operations, let us first consider the inversion symmetry operator \mathcal{I} , acting on $\hat{H}_t \rightarrow \hat{H}_t' = \mathcal{I} \hat{H}_t \mathcal{I}^\dagger$ with

$$\hat{H}_t' = -t \sum_j \left(\hat{b}_{j+1}^\dagger \hat{b}_j e^{i\theta \hat{n}_{j+1}} + e^{-i\theta \hat{n}_{j+1}} \hat{b}_j^\dagger \hat{b}_{j+1} \right). \quad (8)$$

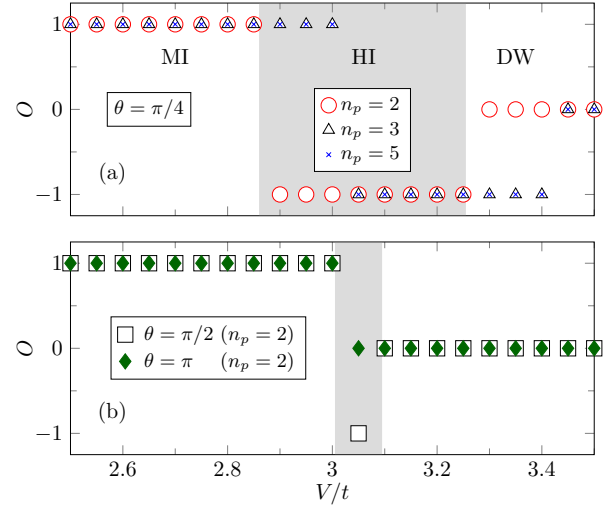


FIG. 1. (Color online). Order parameter O , defined by (14), selecting the topological state in the EAHM at fixed $U/t = 5$ and $\theta = \pi/4$ for different n_p [panel (a)], and at fixed $\theta = \pi/2$ and π for $n_p = 2$ [panel (b)]. Data obtained by iDMRG using with a (relatively small) bond dimension $\chi = 100$.

Applying next a time-reversal transformation \mathcal{T} , $\hat{H}_t' \rightarrow \hat{H}_t'' = \mathcal{T} \hat{H}_t' \mathcal{T}^{-1}$, we obtain

$$\hat{H}_t'' = -t \sum_j \left(\hat{b}_{j+1}^\dagger \hat{b}_j e^{-i\theta \hat{n}_{j+1}} + e^{i\theta \hat{n}_{j+1}} \hat{b}_j^\dagger \hat{b}_{j+1} \right). \quad (9)$$

In order that \hat{H}_t stays invariant under the combined symmetry operations, we take the following transformation into account:

$$\hat{b}_j^\dagger \rightarrow e^{i\theta \hat{n}_j (\hat{n}_j - 1)/2} \hat{b}_j^\dagger e^{-i\theta \hat{n}_j (\hat{n}_j - 1)/2} = \hat{b}_j^\dagger e^{i\theta \hat{n}_j}, \quad (10)$$

$$\hat{b}_j \rightarrow e^{i\theta \hat{n}_j (\hat{n}_j - 1)/2} \hat{b}_j e^{-i\theta \hat{n}_j (\hat{n}_j - 1)/2} = e^{-i\theta \hat{n}_j} \hat{b}_j. \quad (11)$$

Since the second term of Eq. (9) transforms as $e^{i\theta \hat{n}_{j+1}} \hat{b}_j^\dagger \hat{b}_{j+1} \rightarrow \hat{b}_j^\dagger \hat{b}_{j+1} e^{i\theta \hat{n}_j}$, it is equal to the first term of \hat{H}_t . The Hamiltonian $\hat{H}_{\text{EAHM}}^{(b)}$ is therefore invariant under the transformation

$$\mathcal{K} = e^{i\theta \sum_j \hat{n}_j (\hat{n}_j - 1)/2} \mathcal{I} \mathcal{T}. \quad (12)$$

We now show that the combination of $\mathcal{R}^z = e^{i\pi \sum_j \hat{S}_j^z}$ and \mathcal{K} is related to a symmetry-protected topological phase in the EAHM, and define a corresponding topological order parameter. Following Ref. [23], we use the iMPS representation formed by $\chi \cdot \chi$ complex matrices Γ_j and positive, real, diagonal matrices Λ . The iMPS is assumed to be in the canonical form: $\sum_j \Gamma_j \Lambda^2 \Gamma_j^\dagger = \sum_j \Gamma_j^\dagger \Lambda^2 \Gamma_j = \mathbb{I}$. If a state $|\psi\rangle$ is invariant under an internal symmetry which is represented by a unitary matrix $\Sigma_{jj'}$, then the transformed Γ matrices can be shown to satisfy [15, 24]

$$\sum_{j'} \Sigma_{jj'} \Gamma_{j'} = e^{i\varphi} U^\dagger \Gamma_j U, \quad (13)$$

where U is a unitary matrix that commutes with the Λ matrices, and $e^{i\varphi}$ is a phase factor. Similar relations hold for time reversal symmetry, inversion symmetry, and a combination of both. In those cases Γ_j on the left-hand side is replaced by its complex conjugate Γ_j^* , its transpose Γ_j^T and its Hermitian transpose Γ_j^\dagger , respectively. The properties of the matrices U can be used to classify symmetry-protected topological phases [15, 25]. For instance, in the case of time reversal or (modified) inversion symmetry the matrices satisfy $U_{\mathcal{T}} U_{\mathcal{T}}^* = \pm \mathbb{1}$ or $U_{\mathcal{I}(\cdot)} U_{\mathcal{I}(\cdot)}^* = \pm \mathbb{1}$, and the sign distinguishes between two symmetric phases. In the EAHM, the situation is slightly different because time reversal and inversion are not symmetries of the system, only a combination \mathcal{K} of them is. For \mathcal{R}^z and \mathcal{K} we have $U_{\mathcal{R}^z}^2 = e^{i\alpha_{\mathcal{R}^z}} \mathbb{1}$ and $U_{\mathcal{K}}^2 = e^{i\alpha_{\mathcal{K}}} \mathbb{1}$. From this we can derive a symmetry-protected topological phase similar to the case of the $Z_2 \times Z_2$ spin rotation symmetry of \mathcal{R}^z and \mathcal{R}^x in the spin-1 XXZ chain [15]. Since the phase factors $e^{i\alpha_{\mathcal{R}^z}}$ and $e^{i\alpha_{\mathcal{K}}}$ can be removed by absorbing them into the corresponding matrices $U_{\mathcal{R}^z}$ and $U_{\mathcal{K}}$ they have no physical meaning. However, if both \mathcal{R}^z and \mathcal{K} are preserved, the combination $\mathcal{R}^z \mathcal{K}$ is a symmetry as well and its phase factor is not arbitrary if $U_{\mathcal{R}^z}$ and $U_{\mathcal{K}}$ have been fixed. Indeed one can show that $U_{\mathcal{R}^z} U_{\mathcal{K}} = \pm U_{\mathcal{K}} U_{\mathcal{R}^z}$ which defines two different phases. To verify that the EAHM has a nontrivial topological phase protected by \mathcal{R}^z and \mathcal{K} , we calculate the order parameter [21]

$$O = \frac{1}{\chi} \text{tr} \left(U_{\mathcal{K}} U_{\mathcal{R}^z} U_{\mathcal{K}}^\dagger U_{\mathcal{R}^z}^\dagger \right), \quad (14)$$

if the state is symmetric under both \mathcal{K} and \mathcal{R}^z . Otherwise, if one of the symmetries is broken, the order parameter is zero. The iDMRG results for the order parameter are shown in Fig. 1.

If $U_{\mathcal{K}}$ and $U_{\mathcal{R}^z}$ commute ($O = 1$), the system is in a trivial phase, i.e., a site-factorizable MI state, whereas if they anticommute ($O = -1$), the system realizes a nontrivial Haldane phase. Increasing the number of particles per site n_p at fixed $U/t = 5$, the HI phase ($O = -1$) slightly shifts to larger value of V/t but, most notably, the Haldane phase still occupies a solid parameter region, see data for $n_p = 3$ and 5 in Fig. 1(a). Increasing the fractional angle θ for $n_p = 2$, the Haldane state region narrows and finally disappears for $\theta = \pi$ (compare the data presented in Fig. 1(b) for $\theta = \pi/2$). We like to emphasize that the HI sector marked in Fig. 1 by the gray area agrees with that extracted from the correlation length, the entanglement spectrum, and the numerically obtained central charge [26].

Figure 2 represents the ground-state phase diagram of the 1D EAHM in the V - U plane, as obtained from large-scale (i)DMRG calculations for $\theta = \pi/4$ and $n_p = 2$. The phase boundaries are determined simulating the order parameter O , as well as the correlation length and the entanglement spectrum [26]. The EAHM exhibits

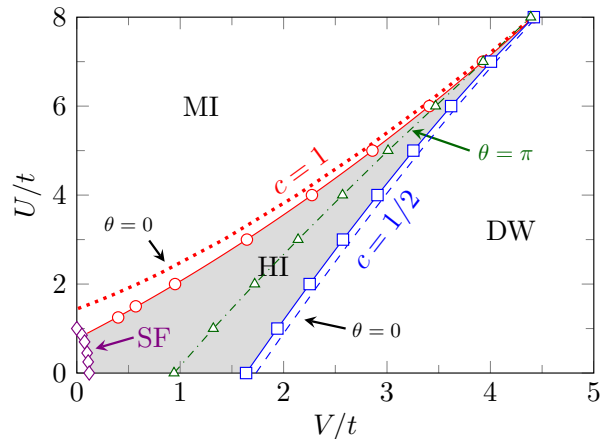


FIG. 2. (Color online). Ground-state phase diagram of the extended anyon-Hubbard model in one dimension, where the particle density $\rho = 1$, $n_p = 2$, and $\theta = \pi/4$. Most notably the Haldane insulator (HI), located between Mott insulator (MI) and density wave (DW) insulating phases in the EBHM, survives for any $\theta > 0$, i.e., in the anyonic case. Likewise the superfluid (SF) appears in the very weak-coupling regime. The MI-HI (squares) and HI-DW (circles) transition points can be determined by a divergent correlation length ξ_χ as χ increases, i.e., the model becomes critical with the central charge $c = 1$ and $c = 1/2$, respectively (see [26]). For comparison, the dotted (dashed) line marks the MI-HI (HI-DW) transition in the EBHM ($\theta = 0$) [27]. The dash-dotted line with triangles up denotes the first-order MI-DW phase transition for $\theta = \pi$.

three different insulating phases (MI, DW, and HI) and a superfluid state in the weak interaction regime, just as for the EBHM [27] but with the addition that the region of the intervening anyonic HI phase at $\theta = \pi/4$ is slightly reduced. The HI will disappear in the pseudofermionic case ($\theta = \pi$). The MI-HI and HI-DW quantum phase transitions belong to the universality class of Tomonaga-Luttinger liquid and Ising model, with central charge $c = 1$ and $1/2$, respectively, see Fig. S1(c) in [26].

Perhaps the most striking feature of the AHM is the asymmetry of the momentum distribution function in k -space [12, 13]. The position of the maximum strongly depends on the fractional phase θ [remind that the momentum distribution diverges at $k = 0$ in the Bose-Hubbard model ($\theta = 0$)]. We expect that this asymmetry can also be observed in dynamical quantities such as the dynamical structure factor $S(k, \omega)$. Hence, if an anyonic system will be realized in optical lattices, $S(k, \omega)$ might be one of the best physical quantities to look at, comparing theoretical predictions with real experiments, like for 1D Bose-Hubbard type models [28]. $S(k, \omega)$ should be easily accessible by momentum resolved Bragg spectroscopy [29]. Furthermore, it has been recently demonstrated that $S(k, \omega)$ can also be used to distinguish the topological HI from the conventional MI and DW states [27, 30], in analogy to exploiting the dynamical

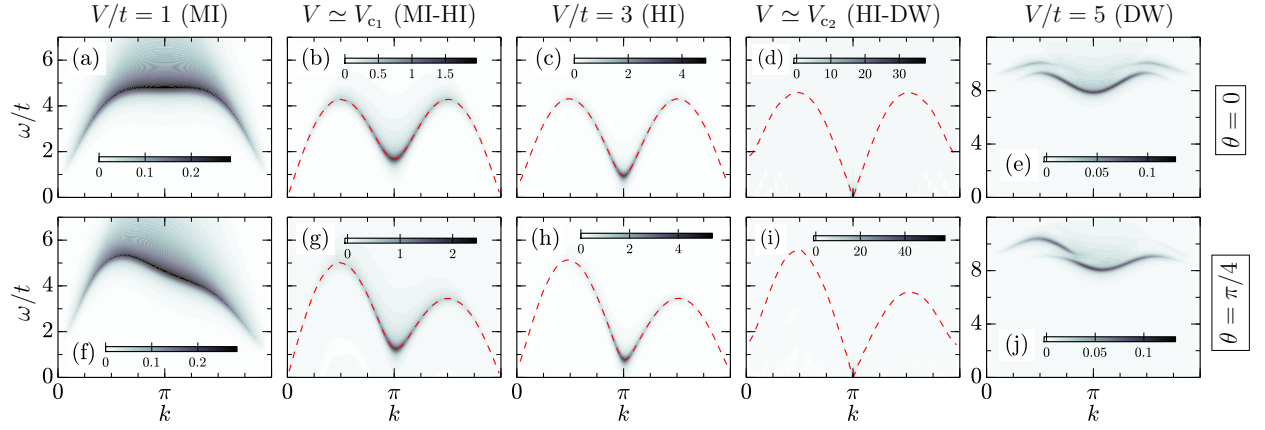


FIG. 3. (Color online). Intensity plots of the dynamical structure factor $S(k, \omega)$ in the EBHM ($\theta = 0$; upper panels) and in the EAHM ($\theta = \pi/4$; lower panels) for characteristic values of V/t at fixed $U/t = 5$. Again the maximum number of particles per site is limited to $n_p = 2$. Dashed lines in panels (b)-(d) and (g)-(i) mark the highest intensity of $S(k, \omega)$ in the k - ω plane.

spin-spin structure factor in the spin-1 XXZ chain [31].

The dynamical density structure factor is defined as

$$S(k, \omega) = \sum_n |\langle \psi_n | \hat{n}_k | \psi_0 \rangle|^2 \delta(\omega - \omega_n), \quad (15)$$

where $|\psi_0\rangle$ ($|\psi_n\rangle$) denotes the ground (n th excited) state and $\omega_n = E_n - E_0$. To compute this quantity, we follow Ref. [32] and first determine the two-point correlation function $\langle \psi_0 | \hat{n}_j(\tau) \hat{n}_0(0) | \psi_0 \rangle$ by real-time evolution of the iMPS $|\psi_0\rangle$. Fourier transformation then provides us with accurate numerical results of the dynamical structure factor in the EAHM.

Figure 3 compares the intensity of the dynamical wave-vector-resolved density response in the EBHM ($\theta = 0$) with those in the EAHM for $\theta = \pi/4$, for $U/t = 5$, at five characteristic V/t -values. One point worthy of remark is that each of the phases and phase transitions can be distinguished by looking at $S(k, \omega)$. In the MI, at $V = t$ [Fig. 3(a) and (f)], the excitation gap appears at $k \approx 0$. With increasing V/t , the MI-HI transition occurs at $V \simeq V_{c1}$, where the excitation gap closes at $k = 0$ as shown in Fig. 3(b) and (g). Deep in the HI phase, $V = 3t$ [Fig. 3(c) and (h)], the spectral weight exclusively concentrates at $k \simeq \pi$ and there are finite excitation gaps at $k = 0$ and π . It is of particular interest to see whether the gap $S(k, \omega)$ closes at the HI-DW transition point. Indeed, the excitation gap at $V = V_{c2}$ closes, but at momentum $k = \pi$, reflecting the lattice-period doubling in the DW phase. Moreover, in the DW phase [Fig. 3(e) and (j)], we find a large excitation gap at $k = \pi$ and two dispersive branches, where a changeover of the intensity maximum occurs at $k = \pi/2$ ($k = 3\pi/4$) for $\theta = 0$ ($\theta = \pi/4$). Interestingly, the influence of the occupation-dependent phase of \hat{H}_t in (5) shows up in $S(k, \omega)$ as well, which helps to differentiate the results from those of the EBHM. $S(k, \omega)$ of the EAHM is asymmetric for any $0 < \theta < \pi$,

while $S(k, \omega)$ in the EBHM is always symmetric about $k = \pi$.

To summarize, we carried out an unbiased numerical investigation of the extended anyon-Hubbard model in one dimension and determined its ground-state phase diagram with high precision exploiting the behavior of correlation lengths and entanglement spectra. Defining an order parameter that distinguishes trivial and nontrivial topological phases, we were able to show that the EAHM possesses an anyonic Haldane insulator state sandwiched between superfluid, Mott insulator and density-wave phases. Both the HI-MI and HI-DW quantum phase transitions are critical with central charge 1 and 1/2, respectively. While the HI state survives the EBHM limit ($\theta = 0$), it vanishes when the system is composed of pseudofermions ($\theta = \pi$). If an 1D interacting anyonic system could be realized experimentally in the future, maybe in an optical-lattice setup with ultracold atoms, we suggest performing momentum-resolved Bragg spectroscopy to look for the pronounced asymmetry of the density response spectra in momentum space which we have demonstrated in our model calculation theoretically.

The iDMRG simulations were performed using the ITensor library [33]. This work was supported by Deutsche Forschungsgemeinschaft (Germany), SFB 652, project B5.

-
- [1] J. M. Leinaas and J. Myrheim, *Nuovo Cimento B* **37**, 1 (1977).
 - [2] F. Wilczek, *Phys. Rev. Lett.* **49**, 957 (1982).
 - [3] D. C. Tsui, H. L. Stormer, and A. C. Gossard, *Phys. Rev. Lett.* **48**, 1559 (1982).
 - [4] R. B. Laughlin, *Phys. Rev. Lett.* **50**, 1395 (1983).
 - [5] F. D. M. Haldane, *Phys. Rev. Lett.* **67**, 937 (1991).

- [6] I. Bloch, J. Dalibard, and W. Zwerger, *Rev. Mod. Phys.* **80**, 885 (2008).
- [7] T. Keilmann, S. Lanzmich, I. McCulloch, and M. Roncaglia, *Nat. Commun.* **2**, 361 (2011).
- [8] S. Greschner and L. Santos, *Phys. Rev. Lett.* **115**, 053002 (2015).
- [9] C. Sträter, S. C. L. Srivastava, and A. Eckardt, *Phys. Rev. Lett.* **117**, 205303 (2016).
- [10] A. Kundu, *Phys. Rev. Lett.* **83**, 1275 (1999).
- [11] J. Arcila-Forero, R. Franco, and J. Silva-Valencia, *Phys. Rev. A* **94**, 013611 (2016).
- [12] Y. Hao, Y. Zhang, and S. Chen, *Phys. Rev. A* **79**, 043633 (2009).
- [13] G. Tang, S. Eggert, and A. Pelster, *New J. Phys.* **17**, 123016 (2015).
- [14] Z.-C. Gu and X.-G. Wen, *Phys. Rev. B* **80**, 155131 (2009).
- [15] F. Pollmann, A. M. Turner, E. Berg, and M. Oshikawa, *Phys. Rev. B* **81**, 064439 (2010).
- [16] E. G. Dalla Torre, E. Berg, and E. Altman, *Phys. Rev. Lett.* **97**, 260401 (2006).
- [17] E. Berg, E. G. Dalla Torre, T. Giamarchi, and E. Altman, *Phys. Rev. B* **77**, 245119 (2008).
- [18] F. Wilczek, *Fractional Statistics and Anyon Superconductivity* (World Scientific, 1990).
- [19] S. R. White, *Phys. Rev. Lett.* **69**, 2863 (1992).
- [20] U. Schollwöck, *Ann. Phys.* **326**, 96 (2011).
- [21] F. Pollmann and A. M. Turner, *Phys. Rev. B* **86**, 125441 (2012).
- [22] I. P. McCulloch, arXiv:0804.2509.
- [23] G. Vidal, *Phys. Rev. Lett.* **98**, 070201 (2007).
- [24] D. Pérez-García, M. M. Wolf, M. Sanz, F. Verstraete, and J. I. Cirac, *Phys. Rev. Lett.* **100**, 167202 (2008).
- [25] X. Chen, Z.-C. Gu, and X.-G. Wen, *Phys. Rev. B* **84**, 235128 (2011).
- [26] Supplementary material.
- [27] S. Ejima, F. Lange, and H. Fehske, *Phys. Rev. Lett.* **113**, 020401 (2014).
- [28] D. Clément, N. Fabbri, L. Fallani, C. Fort, and M. Inguscio, *Phys. Rev. Lett.* **102**, 155301 (2009).
- [29] P. T. Ernst, S. Götze, J. S. Krauser, K. Pyka, D.-S. Lühmann, D. Pfannkuche, and K. Sengstock, *Nat. Phys.* **6**, 56 (2010).
- [30] S. Ejima and H. Fehske, *J. Phys.: Conf. Ser.* **592**, 012134 (2015).
- [31] S. Ejima and H. Fehske, *Phys. Rev. B* **91**, 045121 (2015).
- [32] H. N. Phien, G. Vidal, and I. P. McCulloch, *Phys. Rev. B* **86**, 245107 (2012).
- [33] <http://itensor.org/>.

Supplementary material

As discussed in the main text, we find compelling evidence for the existence of the symmetry-protected topological Haldane insulator phase in the one-dimensional (1D) extended anyon-Hubbard model (EAHM), by calculating an order parameter from the largest eigenvalues of the generalized transfer matrix within an infinite density-matrix renormalization group (iDMRG) scheme.

Here we show that for the EAHM (with maximum number of particles per site $n_p = 2$) further quantities can be exploited in order to determine and characterize the phase boundaries and quantum phase transitions with high precision.

The entanglement analysis in particular provides us with valuable information about the existence of a symmetry protected Haldane insulator (HI) in the EAHM. Furthermore, it allows to determine the phase boundaries between the HI and other insulating phases. Dividing a system into two subblocks, $\mathcal{H} = \mathcal{H}_L \otimes \mathcal{H}_R$, and considering the reduced density matrix $\rho_L = \text{Tr}_R[\rho]$, the entanglement spectra [S1] can be extracted from the singular values λ_α of ρ_L as $\epsilon_\alpha = -2 \ln \lambda_\alpha$. In addition, the correlation length ξ_χ can be obtained from the second largest eigenvalue of the transfer matrix for some fixed bond dimension χ in an iDMRG simulation [S2, S3]. While ξ_χ stays finite as a consequence of the fixed bond dimension χ , the physical correlation length will diverge at the critical point. Nevertheless, ξ_χ is useful to pinpoint a phase boundary because it rapidly increases with χ close to the quantum phase transition point.

Figures S1(a) and (b) show ξ_χ and ϵ_α as functions of V/t for fixed $U/t = 5$. The strong upturn of ξ_χ indicates the formation of a HI phase in the EAHM for $\theta > 0$. We find distinct peaks at $V_{c1} \simeq 2.859t$ and $V_{c2} \simeq 3.255t$, which become more pronounced as χ grows from 100 to 200, signaling a divergence of $\xi_\chi \rightarrow \infty$ as $\chi \rightarrow \infty$. At the same time, the entanglement spectra develops a characteristic double degeneracy in all entanglement levels for $V_{c1} < V < V_{c2}$, indicating a symmetry-protected topological phase between MI and DW states.

The universality class of these quantum phase transitions can be explored by calculating the central charge numerically, just as in case of the EBHM [S4]. When the system gets critical the central charge can be determined very accurately by DMRG, utilizing the relation [S5]

$$c^*(L) \equiv \frac{3[S_L(L/2 - 1) - S_L(L/2)]}{\ln[\cos(\pi/L)]}. \quad (\text{S1})$$

In this way, the MI-SF transition in the BHM [S6], and especially, the universality class of the MI-HI and HI-DW quantum phase transitions in the EBHM have been de-

termined in the past [S4].

Figure S1(c) displays $c^*(L)$ for the 1D EAHM, where the model parameters are the same as in Figs. S1(a) and (b). Running the DMRG we adopt periodic boundary

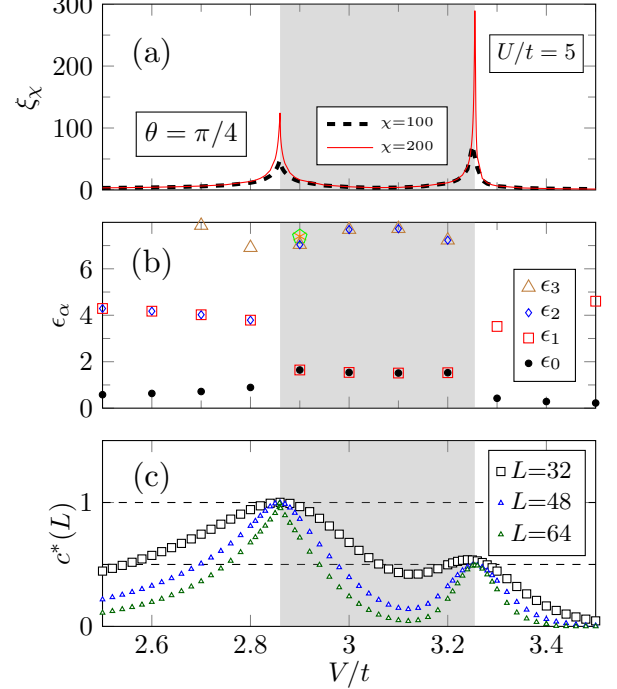


FIG. S1. (Color online). Correlation length ξ_χ [panel (a)] and entanglement spectrum ϵ_α [panel (b)] as a function of V/t for $U/t = 5$ and $\theta = \pi/4$ from iDMRG. Panel (c) displays the central charge $c^*(L)$ for the same parameter set, signaling a MI-HI (HI-DW) quantum phase transition with $c = 1$ ($c = 1/2$). Here data obtained by the finite-system DMRG with periodic boundary conditions.

conditions for system sizes up to $L = 64$. For $U/t = 5$ and $V \simeq V_{c1}$ [$V \simeq V_{c2}$], we find $c^*(L = 64) \simeq 0.996$ [$c^*(L = 64) \simeq 0.494$], which points to the universality class of the Luttinger liquid (Ising) model, in accordance with what was obtained for the corresponding quantum phase transitions in the EBHM ($\theta = 0$).

-
- [S1] H. Li and F. D. M. Haldane, Phys. Rev. Lett. **101**, 010504 (2008).
[S2] I. P. McCulloch, arXiv:0804.2509.
[S3] U. Schollwöck, Ann. Phys. **326**, 96 (2011).
[S4] S. Ejima, F. Lange, and H. Fehske, Phys. Rev. Lett. **113**, 020401 (2014).
[S5] S. Nishimoto, Phys. Rev. B **84**, 195108 (2011).
[S6] S. Ejima, H. Fehske, F. Gebhard, K. zu Münster, M. Knap, E. Arrigoni, and W. von der Linden, Phys. Rev. A **85**, 053644 (2012).